Detecting sublunar-mass primordial black holes with the Earth-Moon binary system

Ya-Ling Li,[1,2] Guo-Qing Huang,[1,2,*] Zong-Qiang Huang,[1,2] and Fu-Wen Shu[1,2,3,4,†]

[1]*Department of Physics, Nanchang University, Nanchang 330031, China*
[2]*Center for Relativistic Astrophysics and High Energy Physics, Nanchang University, Nanchang 330031, China*
[3]*GCAP-CASPER, Physics Department, Baylor University, Waco, Texas 76798-7316, USA*
[4]*Center for Gravitation and Cosmology, Yangzhou University, Yangzhou 225009, China*

(Received 4 October 2022; accepted 26 March 2023; published 11 April 2023)

In this paper we propose a new way to detect sublunar-mass primordial black holes (PBHs) by direct observations of the Earth-Moon binary system. Our method is based on treating PBH as a perturbation term, by assuming that the PBH is sweeping across the Solar System with a sublunar mass and is far away from the Earth-Moon binary (much greater than 1 AU). This perturbation treatment allows us to develop a framework to calculate the orbits of a generic binary system such as the Earth-Moon binary system. Our numerical results show that the Earth-Moon distance is sensitive to the initial values of the system. In most cases, the long-duration interactions between the PBH and the Earth-Moon system can induce lasting imprints on the Earth-Moon's orbit, and these imprints can accumulate over time, eventually giving rise to observable deviations which can be used to infer the properties of the PBH.

DOI: 10.1103/PhysRevD.107.084019

I. INTRODUCTION

Astrophysical and cosmological observations provide convincing evidence that more than one quarter of the total energy density of the Universe is in the form of cold and weakly interacting matter, the dark matter (DM) [1–4]. The experimental and theoretical searching for particle DM has lasted for several decades and a great deal of well-motivated particle DM candidates have been proposed. However, as the parameter space of particle DM models becomes tighter and tighter constrained by experiments [5,6], more and more nonparticle candidates are coming into view. Among them primordial black holes (PBHs) as a candidate that could contribute a fraction of DM have attracted considerable attention in the past years. The research on PBHs could trace back to the 1960s, which was initiated by Zel'dovich and Novikov [7], and developed by Hawking and Carr [8–10]. It was generally believed that they could have been formed in the early Universe via the collapse of large density perturbations. Various mechanisms have been proposed to create such black holes in the past years [11–42]. Most mechanisms predict that the mass of PBHs may exist in a wide range, from $\sim 10^{14}$ g (below which they would have been evaporated completely via the Hawking radiation), to tens of thousands of solar masses. Hence, PBHs are a good candidate in explaining the origin of the black holes that cannot be formed in standard astrophysical processes, for instance, the intermediate mass black holes as recently observed by LIGO [43,44].

Various techniques have been developed in order to probe PBHs in a large range of masses in the past decades [45–49]. This process was further accelerated by the direct detection of gravitational waves [50,51]. Up to now, there are numerous observational constraints on the fraction of DM comprised of PBHs, see [52–79] for an incomplete list. However, there still exist wide windows (masses from 10^{16} to 10^{21} g) where PBHs can form whole or a significant fraction of the DM. It is extremely difficult to detect these PBHs in a direct way, considering that they are only of atomic size. Despite all this, there are proposals that try to detect them in an indirect way. More specifically, these schemes consider that these PBHs are captured by neutron stars (NSs) or white dwarfs in dwarf galaxies [80–82]. It is generally believed that once a PBH is captured by a NS, the NS would be accreted onto the PBH such that the NS gets destroyed in a much shorter time than its normal lifetime. Hence, observations of NSs, in turn, will effectively impose constraints on the abundance of PBHs. This method, very recently, has been extended to the capture of PBHs by main sequence, Sun-like stars [83], which have the advantage, as compared to NS and white dwarfs, that they can be observed in dwarf galaxies more frequently. However, these methods are model dependent, and, as mentioned before, are indirect.

*huanggq@ncu.edu.cn
†shufuwen@ncu.edu.cn

This motivates us to explore alternatives that can overcome these flaws. One possibility is to study the interaction between PBHs and astronomical binary systems, for instance, the Earth-Moon binary system, which has been studied for tens of centuries and is of the most accurate detections among all astronomical binary systems. The idea is simple. As PBHs pass nearby the Solar System, the long-duration interactions between PBHs and the Earth-Moon system could leave lasting imprints on the Earth-Moon's orbit. As the interactions continue, these imprints can accumulate over time, eventually giving rise to observable deviations which can be used to infer the properties of PBHs. Based on this idea, in this work we propose a new way to detect these sublunar-mass PBHs by direct observations of the Earth-Moon system. By treating PBHs as a perturbative term, we also develop a new formalism for calculating the PBH-induced evolution of an astronomical binary system like the Earth-Moon system.

It is helpful to note that our proposal only focuses on PBHs sweeping past the Solar System rather than lurking within it, as sketched in Fig. 1. Since the Solar System is a stable bound system, the perturbations caused by other celestial bodies can be considered as background noise for the Earth-Moon binary system. In our calculations, we subtract the background noise from the deviation of the Moon's orbit caused by the PBH sweeping across the Solar System, which we represent as Δr. Since the population of PBHs near the Solar System is generally very low. Actually, even under the most favorable scenario of PBH DM ($\rho \approx 0.3$ GeV/cm^3) and considering a solar system with a radius of 100 AU, the upper bound on the expected probability of a 10^{20} kg PBH sweeping past the Solar System is approximately 0.16 per year (for more details, please refer to the conclusion section of this paper). Thus, the rate of a PBH sweeping across the Solar System is low, roughly speaking, about one case every six years. This means that the background noise can be readily deduced from the lunar laser ranging (LLR) data. In summary, we determine Δr by subtracting the LLR data from the year when the PBH sweeps across the Solar System from the LLR data of the year when it does not.

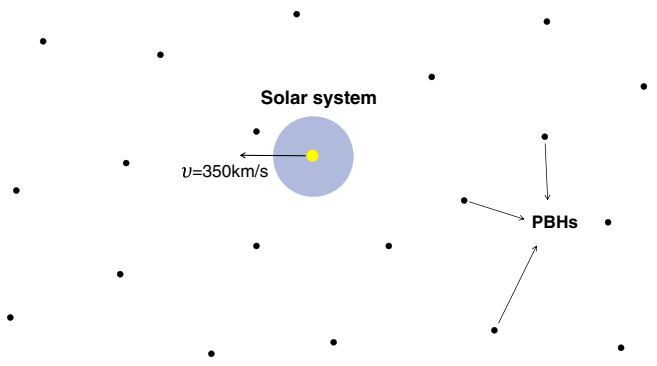

FIG. 1. Sketch of PBHs sweeping across the Solar System. As the Solar System rotates around the Galactic Center, PBH, as a candidate of dark matter, will sweep past the Solar System with a relative velocity $v \sim 350$ km/s [53].

The remainder of this paper is organized as follows. In Sec. II we give a brief review on the osculating orbital elements and the perturbed Kepler problem. In Sec. III we compute the evolution of the osculating orbital elements of a binary system due to the influence of the perturbing force produced by the PBH. In this section, we establish a model of the perturbed two-body problem to detect the PBH. In Sec. IV we show our numerical results for different initial conditions. We summarize our main results in the last section.

II. FORMALISM

In this section we would like to study the osculating orbital elements and the perturbed Kepler problem. We begin by briefly reviewing the fundamental properties of Keplerian orbits, and then introducing the description of Keplerian orbits in space relative to a reference frame and the equations of motion for the osculating orbital elements in the perturbed Kepler problem.

A. Keplerian orbits

The Keplerian orbits are determined by considering the motion of two bodies interacting only within the framework of the Newtonian gravity, and assuming that each body is taken to be spherically symmetric. The equation of motion is given by

$$\ddot{\mathbf{r}} = -\frac{\mu}{r^3}\mathbf{r}, \tag{1}$$

where $\mu = GM_{\rm tot} = G(m_0 + m_1)$ and $r = |\mathbf{r}|$, with G being the universal gravitational constant, $M_{\rm tot}$ being the total mass, and $\mathbf{r}$ being the position vector from m_0 to m_1.

Equation (1) indicates that the force is radial, which implies $\mathbf{r} \times \ddot{\mathbf{r}} = \mathbf{d}(\mathbf{r} \times \dot{\mathbf{r}})/dt = 0$. As a consequence, $\mathbf{H} \equiv \mathbf{r} \times \dot{\mathbf{r}}$ is a constant vector. The constancy of $\mathbf{H}$ has two direct results: One is that the motion is constrained in the orbital plane, a fixed plane which is normal to $\mathbf{H}$. The second is that the magnitude of the vector can be written as

$$H = r^2\dot{\theta}, \tag{2}$$

where θ is the position angle measured from some fixed line in the plane.

With the help of Eq. (2), one can get the shape of the orbit by solving the radial portion of Eq. (1). The solution of Eq. (1) is given by [84]

$$r = \frac{a(1-e^2)}{1 + e\,\cos f}, \tag{3}$$

where e is the eccentricity, and $f = \theta - \omega$ is the true anomaly, with ω being the argument of pericenter. Since ω

is constant, the relation between the angle f and time is given by Eq. (2),

$$\frac{df}{dt} = \frac{H}{r^2}. \tag{4}$$

According to Kepler's third law, we can get the relation between the period and the semimajor axis,

$$\frac{2\pi}{P} = \sqrt{\frac{\mu}{a^3}}, \tag{5}$$

where P is the period, and a is the semimajor axis of the elliptical orbit.

B. Keplerian orbits in space

Let us first introduce a fundamental frame with coordinates (X, Y, Z) and an orbital frame with coordinates (x, y, z) as shown in Fig. 2. In the fundamental (X, Y, Z) frame, let us adopt the $X-Y$ plane as a reference plane, with the Z axis as a reference direction. We also assign a constant vectorial basis $\mathbf{e}_X$, $\mathbf{e}_Y$ and $\mathbf{e}_Z$ to the fundamental frame. In the orbital (x, y, z) frame, the x-y plane is the orbital plane of two-body motion, the x direction is the radial direction of m_1 relative to m_0, and the z direction is aligned with the angular-momentum vector. The orbital frame comes with time-dependent basis vectors $\mathbf{e}_x$, $\mathbf{e}_y$ and $\mathbf{e}_z$. The orientation of the elliptical orbit relative to the fundamental (X, Y, Z) frame is represented by the longitude of ascending node Ω, the inclination i and the argument of pericenter ω.

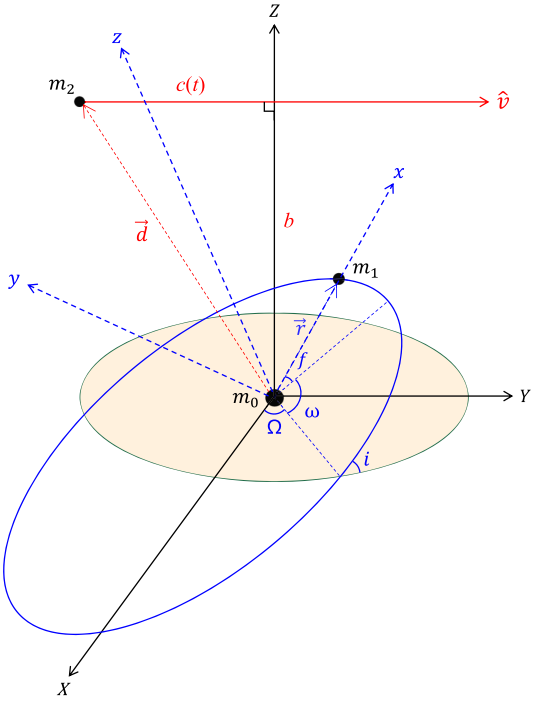

FIG. 2. Schematic picture of the model for detecting PBH with the Earth-Moon binary system. m_0, m_1, m_2 denote the Earth, the Moon, and the PBH, respectively. The elliptical orbit of m_1 is described by the blue line in the figure. The trajectory of the m_2 is described by the solid red line, which always falls on the Y-Z plane and parallels to the Y axis. $\mathbf{d} = c(t)\mathbf{e}_Y + b\mathbf{e}_Z$ is the position vector from m_0 to m_2, with $c(t)$ and b being the components of $\mathbf{d}$ on the Y axes and Z axes, respectively. $\mathbf{v}$ is the velocity vector of the m_2 and $\mathbf{r}$ is the position vector from m_0 to m_1.

With these definitions and conventions, we can go from the orbital (x, y, z) frame to the fundamental (X, Y, Z) frame by performing three consecutive Euler rotations,

$$\begin{aligned}\mathbf{e}_X = {} & [\cos\Omega\cos(\omega+f) - \cos i \sin\Omega \sin(\omega+f)]\mathbf{e}_x \\ & + [-\cos\Omega \sin(\omega+f) - \cos i \sin\Omega\cos(\omega+f)]\mathbf{e}_y \\ & + \sin i \sin\Omega \mathbf{e}_z,\end{aligned} \tag{6}$$

$$\begin{aligned}\mathbf{e}_Y = {} & [\sin\Omega\cos(\omega+f) + \cos i \cos\Omega \sin(\omega+f)]\mathbf{e}_x \\ & + [-\sin\Omega \sin(\omega+f) + \cos i \cos\Omega\cos(\omega+f)]\mathbf{e}_y \\ & - \sin i \cos\Omega \mathbf{e}_z,\end{aligned} \tag{7}$$

$$\mathbf{e}_Z = \sin i \sin(\omega+f)\mathbf{e}_x + \sin i \cos(\omega+f)\mathbf{e}_y + \cos i \mathbf{e}_z. \tag{8}$$

Therefore, the elliptical orbit in space can be described in terms of six orbital elements: a, e, i, Ω, ω, M, which are called semimajor axis, eccentricity, inclination, longitude of ascending node, argument of pericenter, and mean anomaly, respectively [85].

C. Osculating orbital elements and the perturbed Kepler problem

Let us return to the two-body problem, but now suppose that the binary is subjected to some small perturbing force [86]. The equation of motion is

$$\ddot{\mathbf{r}} = -\frac{\mu}{r^3}\mathbf{r} + \mathbf{F}, \tag{9}$$

where $\mathbf{F}$ is the perturbing acceleration. We decompose $\mathbf{F}$ as

$$\mathbf{F} = R\mathbf{e}_x + T\mathbf{e}_y + N\mathbf{e}_z, \tag{10}$$

in terms of components R, T and N. Under the action of perturbing acceleration, the binary will deviate from its Keplerian ellipse, causing its orbital elements to vary. We thus treat $(a, e, i, \Omega, \omega, M)$ as functions of time, called the osculating orbital elements.

Following Refs. [87,88], we write the final equations for the osculating orbital elements,

$$\frac{da}{dt} = \frac{2}{n\beta}[\mathrm{R}e \sin f + T(1 + e\cos f)], \tag{11}$$

$$\frac{de}{dt} = \frac{\beta}{na}\left[\mathrm{R}\sin f + T\left(\cos f + \frac{\cos f + e}{1 + e\cos f}\right)\right], \tag{12}$$

$$\frac{di}{dt} = N\frac{\beta}{na}\frac{\cos(\omega+f)}{1+e\,\cos f}, \tag{13}$$

$$\frac{d\Omega}{dt} = N\frac{\beta}{na}\frac{\sin(\omega+f)}{1+e\,\cos f}\csc\, i, \tag{14}$$

$$\frac{d\omega}{dt} = \frac{\beta}{nae}[-\mathrm{R}\cos f + T(1+\gamma)\sin f] - \cos\, i\frac{d\Omega}{dt}, \tag{15}$$

$$\frac{dM}{dt} = n + \frac{\beta^2}{nae}[\mathrm{R}(\cos f - 2\gamma e) - T(1+\gamma)\sin f], \tag{16}$$

with

$$\frac{df}{dt} = \frac{n}{\beta^3}(1+e\,\cos f)^2 + \frac{\beta}{nae}[R\cos f - T(1+\gamma)\sin f], \tag{17}$$

where $\beta = \sqrt{1-e^2}$, $\gamma = \frac{1}{1+e\cos f}$ and $n = \frac{2\pi}{P}$.

III. DETECTING PBH WITH BINARY SYSTEM: THE MODEL

In this section we turn to calculate the evolution of the osculating orbital elements of a binary system due to the influence of the perturbing force produced by a PBH. We first introduce the model for detecting PBH with the Earth-Moon binary system, before obtaining the analytical expression of the perturbing force, and the evolution of the osculating orbital elements with time under different initial conditions by numerical calculation. We also discuss the dependence of the Earth-Moon distance variation Δr on φ, i, Ω, ω, b, and m_2 under different initial conditions.

Let us assume that the mass of the PBH is very small compared to the Earth and the Moon, and the distance of the PBH is very far away from the Earth-Moon binary system, then we can establish a model of the perturbed two-body problem for detecting the PBH, as sketched in Fig. 2. In this model, the Earth is placed as the origin of the frame,[1] the Moon performs the Kepler motion relative to the Earth, and the force of the PBH on the Moon is regarded as a perturbing one.

The perturbing acceleration is then given by

$$\mathbf{F} = \frac{Gm_2(\mathbf{d}-\mathbf{r})}{|\mathbf{d}-\mathbf{r}|^3}, \tag{18}$$

where $\mathbf{r} = r\mathbf{e}_x$ and $\mathbf{d} = c(t)\mathbf{e}_Y + b\mathbf{e}_Z$. Suppose that the observation starts from the moment $c(0) = -100b$, then $c(t) = vt - 100b$ with $v = 350\ \mathrm{km}\cdot\mathrm{s}^{-1}$, which is the typical velocity for halo dark matter relative to the Earth [53]. Since $d(t) = \sqrt{b^2+c(t)^2} \gg r$, $\mathbf{F}$ can be approximated as

$$\mathbf{F} \approx \frac{Gm_2}{d(t)^3}[c(t)\mathbf{e}_Y + b\mathbf{e}_Z - r\mathbf{e}_x]. \tag{19}$$

Substituting Eqs. (6) and (7) into Eq. (19), we have

$$\begin{aligned}\mathbf{F} \approx \frac{Gm_2}{d(t)^3}\{&(c(t)[\sin\Omega\,\cos(\omega+f) + \cos\, i\,\cos\Omega\,\sin(\omega+f)] + b\,\sin\, i\,\sin(\omega+f) - r)\mathbf{e}_x \\ &+ (c(t)[-\sin\Omega\,\sin(\omega+f) + \cos\, i\,\cos\Omega\,\cos(\omega+f)] + b\,\sin\, i\,\cos(\omega+f))\mathbf{e}_y \\ &+ [c(t)(-\sin\, i\,\cos\Omega) + b\,\cos\, i]\mathbf{e}_z\}.\end{aligned} \tag{20}$$

Since $\mathbf{F} = R\mathbf{e}_x + T\mathbf{e}_y + N\mathbf{e}_z$, the components of the perturbing acceleration in the basis vectors ($\mathbf{e}_x$, $\mathbf{e}_y$, $\mathbf{e}_z$) are

$$\begin{aligned}R &= \frac{Gm_2}{d(t)^3}\{c(t)[\sin\Omega\,\cos(\omega+f) + \cos\, i\,\cos\Omega\sin(\omega+f)] + b\,\sin\, i\,\sin(\omega+f) - r\}, \\ T &= \frac{Gm_2}{d(t)^3}\{c(t)[-\sin\,\Omega\,\sin(\omega+f) + \cos\, i\,\cos\,\Omega\,\cos(\omega+f)] + b\,\sin\, i\,\cos(\omega+f)\}, \\ N &= \frac{Gm_2}{d(t)^3}[c(t)(-\sin\, i\,\cos\Omega) + b\,\cos\, i],\end{aligned} \tag{21}$$

where i, Ω and ω are parameters describing elliptical orbit of the Moon. We can change the trajectory of the PBH relative to the Earth-Moon binary system by changing the initial values of i, Ω and ω. Substituting Eq. (21) into Eqs. (11)–(17), we can get the variation of (a, e, i, Ω, ω, M) with time.

Since the orbit under the perturbing force is tangent to the Keplerian ellipse at each moment, and the position and velocity of the particle in the real orbit are consistent with the corresponding point in the osculating orbit at that

[1]We also assume that the center of mass of the binary is on the Earth considering the small mass of the Moon compared to the Earth.

moment, so the relationship between a, e and r still satisfies the two-body motion relationship [Eq. (3)]. Differentiating Eq. (3), we can get the variation of r with time.

IV. NUMERICAL RESULTS

A. When the initial position is coplanar

We first discuss the influence of the perturbing force of the PBH on the Earth-Moon binary system, when the trajectory of the PBH is coplanar to the elliptical orbit of the Moon, as shown in Fig. 3. Throughout the calculations of this subsection, we set the following initial condition: $i = \frac{\pi}{2}$, $\Omega = \frac{\pi}{2}$, $\omega = \frac{\pi}{2}$, $b = 10$ AU and $m_2 = 10^{20}$ kg.

Substituting the initial condition into Eq. (21), the components of the perturbing acceleration are given by

$$R = \frac{Gm_2}{d(t)^3}[c(t)(-\sin f) + b\cos f - r], \tag{22}$$

$$T = \frac{Gm_2}{d(t)^3}[c(t)(-\cos f) - b\sin f], \tag{23}$$

$$N = 0. \tag{24}$$

Plugging them into Eqs. (11) and (12), the rate of change of a and e then becomes

$$\frac{da}{dt} = -\frac{2}{n\beta}\frac{Gm_2}{d(t)^3}[c(t)(e + \cos f) + (re + b)\sin f], \tag{25}$$

$$\frac{de}{dt} = -\frac{\beta}{na}\frac{Gm_2}{d(t)^3}\frac{c(t)[1 + 2e\cos f + \cos^2 f] + [r + be + (re + b)\cos f]\sin f}{1 + e\cos f}. \tag{26}$$

Combined with Eq. (3), evolutions of Δa, Δe, Δr with time are obtained by numerical calculations. The results are shown in Fig. 4. From these figures, we can see that both Δa and Δr are oscillating quasiperiodically over time, and their amplitudes first increase and then decrease. Δe, in contrast, increases and then decreases over time monotonously. It is worth noting that all of them (Δa, Δe and Δr) reach to zero in the end, which means that the perturbing force of PBHs has no long-term effects on the elliptical orbit of the Moon. The significance here can be understood by analyzing Eqs. (3), (25), and (26). First, since the term $\sin f$ is a periodic function with time, its time integral over the total process is equal to zero. Then, since the trajectory of the PBH is symmetrical about the Z axis, the time integral of the term $c(t) = vt - 100b$ over the total process is also equal to zero. Therefore, the time integral of Eq. (25) over the total process will be equal to zero, which means that the semimajor axis of the elliptical orbit does not change in the end. In the same way, we can also understand both Δe and Δr are equal to zero in the end, by analyzing Eqs. (26) and (3).

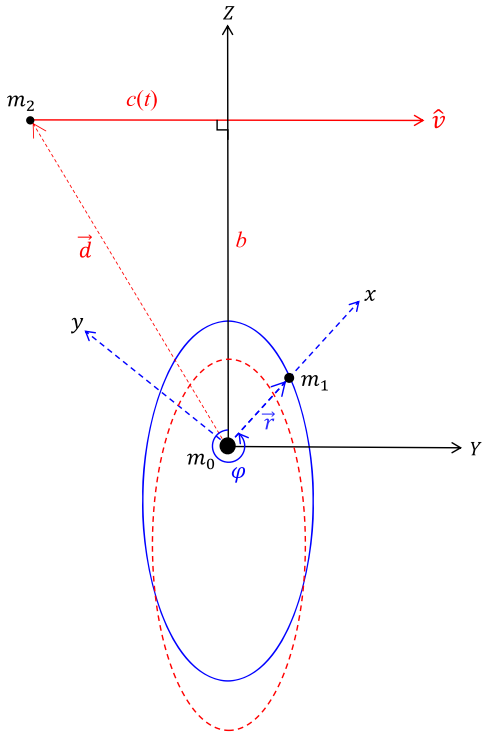

FIG. 3. Schematic diagram when the trajectory of the PBH is coplanar to the elliptical orbit of the Moon. The elliptical orbit of the Moon is depicted by the blue solid line, when $c(t) = -100b$. The elliptical orbit of the Moon is depicted by the red dotted line, when $c(t) = 0$.

In order to quantitatively study the change of the distance between the Earth and the Moon under the perturbing force of PBH, we calculate the evolution of Δr with time under a fixed observation angle φ. The observation angle φ is defined as

$$f = 2m\pi + \varphi, \tag{27}$$

where $m = 0, 1, 2\ldots$ and $\varphi \in [0, 2\pi)$. For instance, $\varphi = 0$ and $\varphi = \pi$ correspond to the moments when the Moon is at perigee and apogee, respectively, which are called "normal points." In the case of $\varphi = 0$, the evolution of the distance between the Earth and the Moon corresponds to make

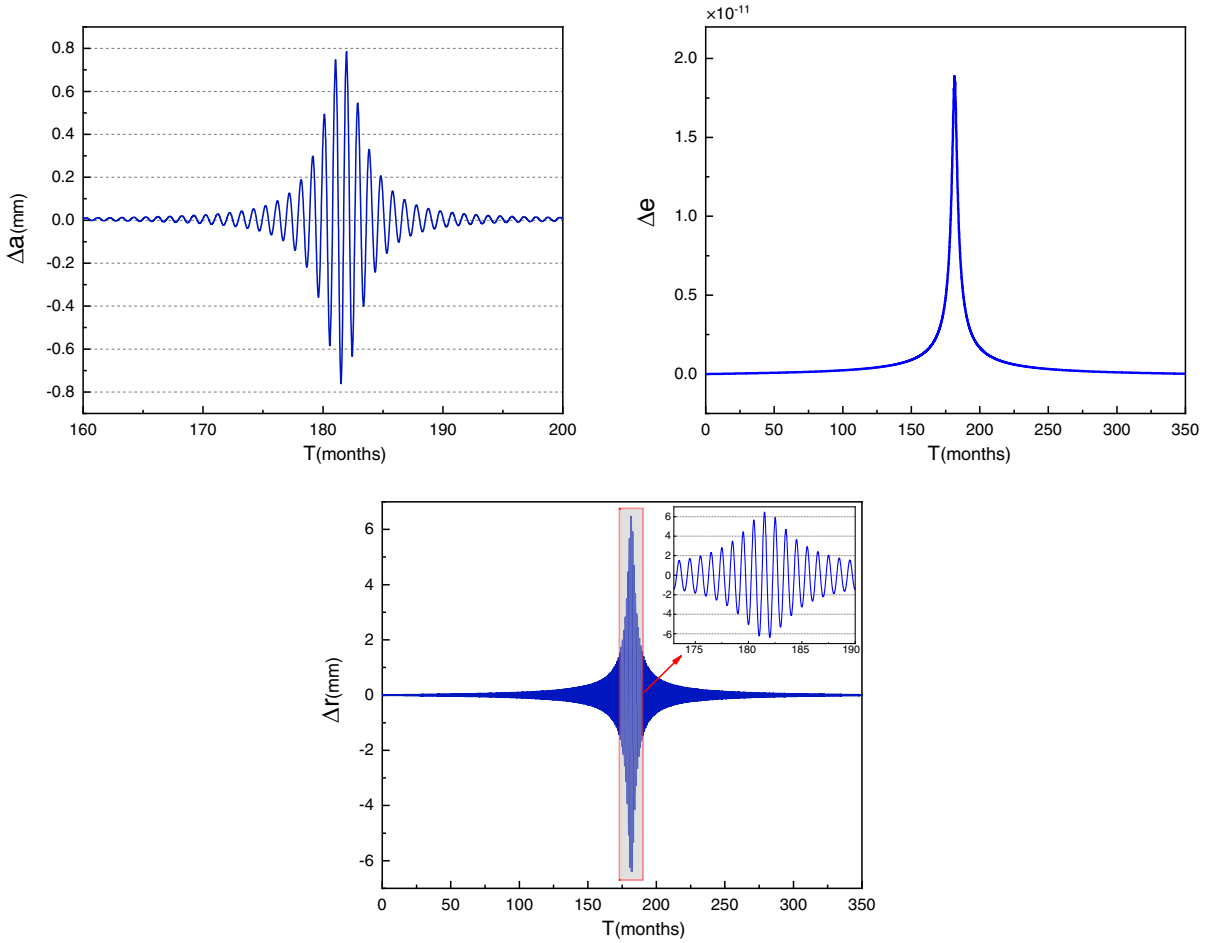

FIG. 4. The evolution of Δa, Δe, Δr with time.

measurements when the Moon is at perigee. The rate of change of a and e in this case are then given by

$$\frac{da}{dt} = -\frac{2}{n\beta}\frac{Gm_2}{d(t)^3}(1+e)c(t), \tag{28}$$

$$\frac{de}{dt} = -\frac{2\beta}{na}\frac{Gm_2}{d(t)^3}c(t). \tag{29}$$

Finally, the evolution of Δr with time can be obtained by numerical calculating Eqs. (3), (28) and (29). The results are presented as the black solid line in Fig. 5. From the black solid line with $\varphi = 0$, we can see that $|\Delta r|$ increases first and then decreases over time monotonously, and reaches a maximum at a certain moment. The significance here can be understood by analyzing the perturbing force of PBH on the Moon. When the Moon is at perigee with $\varphi = 0$ in Fig. 3, the direction of the Moon's velocity is along the negative direction of the Y axis and the perturbing force of PBH on the Moon can be decomposed into the component $R\mathbf{e}_Y$ along Y-axis direction and the component $T\mathbf{e}_Z$ along the Z-axis direction. The component $R\mathbf{e}_Y$ is consistent with the direction of the Moon's velocity when $c(t) < 0$, which causes the Moon's velocity to increase. The greater the velocity, the smaller the orbital radius, according to the law of universal gravitation. The above means that $|\Delta r|$ increases with time when $c(t) < 0$. Similarly, it can be analyzed that the component $R\mathbf{e}_Y$ is opposite to the direction of the Moon's velocity when $c(t) > 0$, which causes $|\Delta r|$ to decrease with time. The component $T\mathbf{e}_Z$ is perpendicular to the direction of the Moon's velocity throughout the process, which does not change the magnitude of the Moon's velocity. Therefore, $|\Delta r|$ increases and then decreases over time monotonously throughout the process, and reaches the maximum when $c(t) = 0$.

In order to quantitatively analyze the relationship between Δr and φ, let us plot the evolution of Δr with time at different observation angles φ as shown in the left panel of Fig. 5, and the dependence of the maximum of Δr on φ as shown in the right panel of Fig. 5. From the right panel of Fig. 5, we can see that Δr acts like a trigonometric function of φ. The value of Δr is equal to zero when φ tends to $\frac{\pi}{2}$ and $\frac{3\pi}{2}$, and $|\Delta r|$ reaches its maximum value ($\approx$6.46 mm) when φ is equal to 0 or π. This means that the greatest change in the distance between

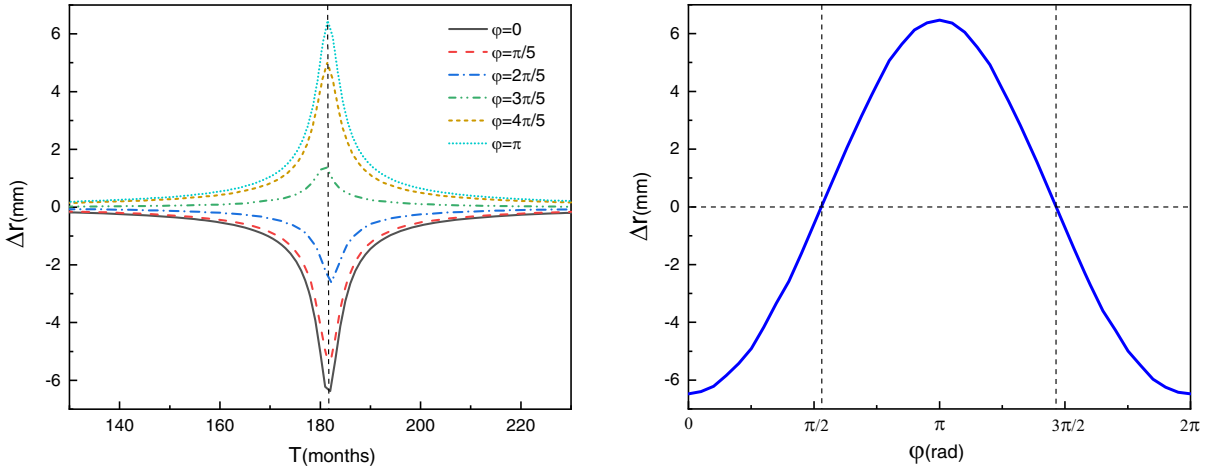

FIG. 5. Left panel: the evolution of Δr with time under different fixed observation angles φ. Right panel: the peak value of $\Delta r(T)$ (i.e., the values of Δr at the dotted line in the figure on the left panel) as a function of φ, which corresponds to the dependence of Δr on φ when $c(t) = 0$.

the Earth and the Moon can be observed by the normal point measurement. Since the current detection accuracy of the Earth-Moon distance can reach the millimeter level [89–92], we can accurately detect PBH with the Earth-Moon binary system, when the system reaches certain initial conditions.

Recalling the change curve of e with time in Fig. 4 and the above analysis, we can roughly speculate that the elliptical orbit of the Moon first moved down as a whole and then moved up back to its initial position over time. The offset and eccentricity of the elliptical orbit reach the maximum when $c(t) = 0$. In the end, we can roughly represent the elliptical orbit of the Moon with the red dotted line in Fig. 3.

In what follows, let us turn to investigate the effects of the perturbing force on the Earth-Moon binary system when the observation angle $\varphi = 0$ under different azimuths, distances and masses of the PBH, which is equivalent to vary a parameter in i, Ω, ω, b, m_2 and keep other parameters unchanged. The details are shown in the left panels of Figs. 6–10. In addition, the dependence of Δr on i, Ω, ω, b, m_2 is presented in the right panels of Figs. 6–10, respectively.

From the left panel in Figs. 6 and 7, we can see that simply changing i has little effect on Δr, while changing Ω (with other parameters fixed) has larger effects on Δr, and Δr can always return to zero in the end, regardless the values of i and Ω. This implies that the perturbing force of

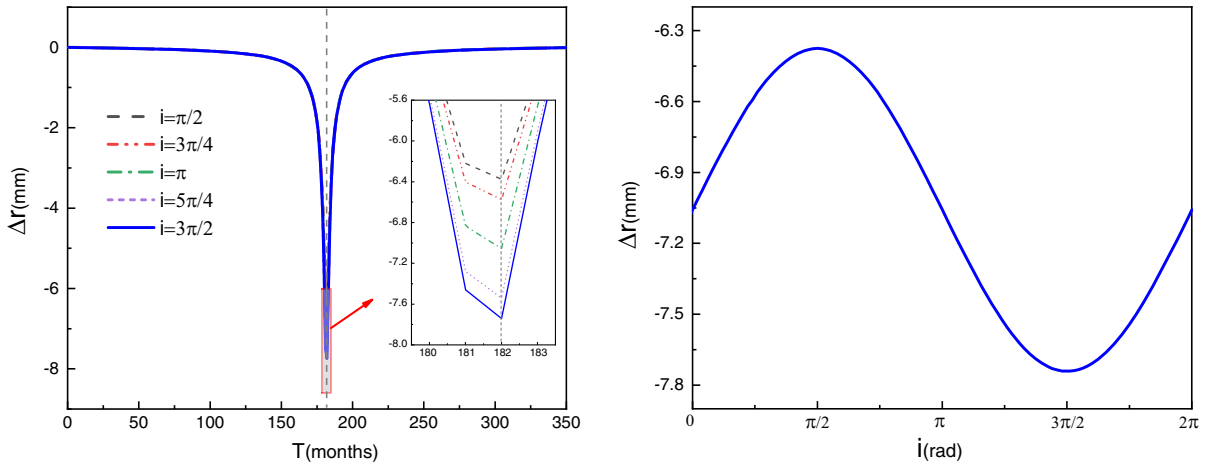

FIG. 6. Left panel: the evolution of Δr over time when $\varphi = 0$ under different i and other parameters fixed. Right panel: the peak value of $\Delta r(T)$ (i.e., the values of Δr at the dotted line in the figure on the left panel) as a function of i, which corresponds to the dependence of Δr on i when $c(t) = 0$.

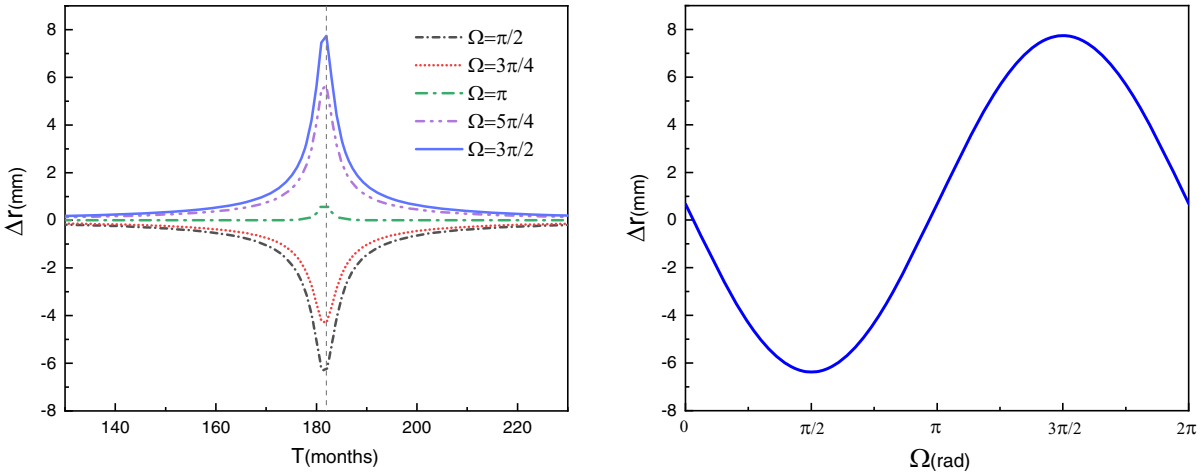

FIG. 7. Left panel: the evolution of Δr with time when $\varphi = 0$ under different Ω and other parameters fixed. Right panel: the peak value of $\Delta r(T)$ (i.e., the values of Δr at the dotted line in the figure on the left panel) as a function of Ω, which corresponds to the dependence of Δr on Ω when $c(t) = 0$.

PBH has no long-term effects on the elliptical orbit of the Moon. From the right panels in Figs. 6 and 7, we can see that Δr acts like a sinusoidal function of i and Ω when $c(t) = 0$, which is consistent with the calculated results in Ref. [93].

Figure 8, however, presents another situation. It can be seen that Δr cannot return to zero for any $\omega \neq \frac{\pi}{2}$ or $\frac{3\pi}{2}$, which means that the perturbing force of PBH will have long-term effects on the elliptical orbit of the Moon. Again Δr acts like a trigonometric function of ω as shown in the right panel in Fig. 8.

The left panel in Fig. 9 shows that the widths of the peaks of the $\Delta r(T)$ curve increase as b increases, which means that the farther the PBH is from Earth, the longer observation time is required. In addition, the peak value of Δr is almost inversely proportional to b, as clearly shown in the right panel of Fig. 9. This means that the farther the PBH from the Earth-Moon binary system is, the smaller the offset of the Moon's elliptical orbit will be.

Finally, let us turn to Fig. 10, which shows that Δr is proportional to m_2, and is consistent with the results in Refs. [94,95]. Therefore, the greater the mass of the PBH is, the greater the offset of the Moon's elliptical orbit will be. Roughly speaking, the heavier the PBHs are, the more possibilities to detect them are. However, PBHs with mass greater than the lunar mass ($\sim 10^{23}$ kg) will make our perturbative calculations breakdown.

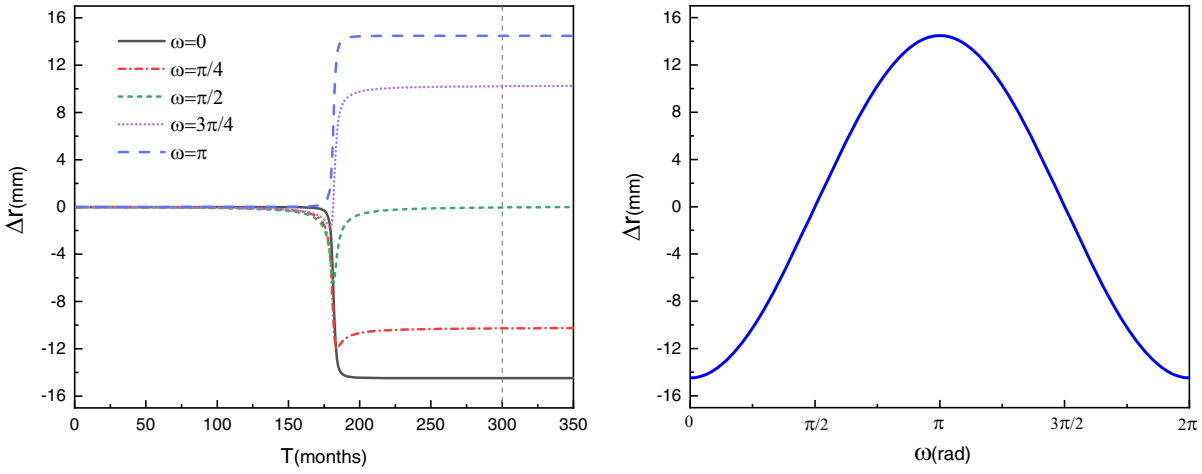

FIG. 8. Left panel: the evolution of Δr with time when $\varphi = 0$ under different ω and other parameters fixed. Right panel: the values of $\Delta r(T = 300)$ at the dotted line in the figure on the left panel as a function of ω, which corresponds to the dependence of Δr on ω when $c(t) = 100b$.

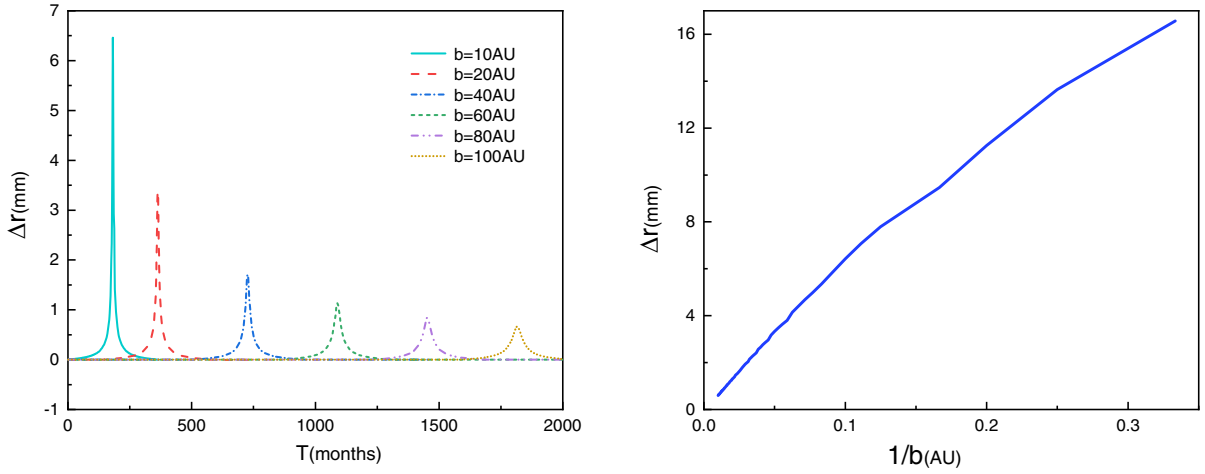

FIG. 9. Left panel: the evolution of Δr with time when $\varphi = \pi$ under different b and other parameters fixed. Right panel: the peak value of $\Delta r(T)$ in the figure on the left panel as a function of b, which corresponds to the dependence of Δr on b when $c(t) = 0$.

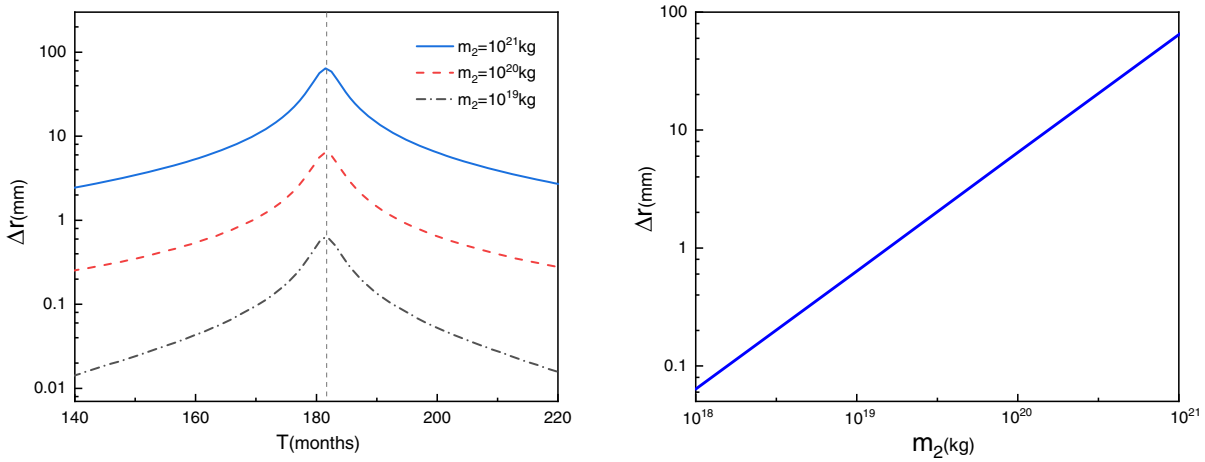

FIG. 10. Left panel: the evolution of Δr with time when $\varphi = \pi$ under different m_2 and other parameters fixed. Right panel: the peak value of $\Delta r(T)$ (i.e., the values of Δr at the dotted line in the figure on the left panel) as a function of m_2, which corresponds to the dependence of Δr on m_2 when $c(t) = 0$.

B. When the initial position is noncoplanar

We now discuss the influence of the perturbing force of the PBH on the Earth-Moon binary system, when the trajectory of the PBH is noncoplanar to the elliptical orbit of the Moon. Throughout the calculations of this subsection, we set the following initial condition: $i = \frac{\pi}{4}$, $\Omega = \frac{\pi}{4}$, $\omega = \frac{\pi}{4}$, $b = 10$ AU and $m_2 = 10^{20}$ kg.

Evolutions of Δa, Δe, Δr with time are shown in Fig. 11. One can see that, after the PBH passes through, the semimajor axis of the orbit remains unchanged, while the eccentricity of the orbit increases which leads to the distance between the Earth and the Moon changing. This means that the perturbing force of PBH has long-term effects on the Earth-Moon binary system.

Comparing Fig. 4 with Fig. 11, we find that Δr is mainly determined by Δe. This result can be explained by analyzing the relationship between Δa, Δe and Δr via Eq. (3). According to Eq. (3), Δr is obtained by

$$\Delta r = \frac{1-e^2}{1+e\cos f}\Delta a + a\left[\frac{-2e(1+e\cos f)-(1-e^2)\cos f}{(1+e\cos f)^2}\right]\Delta e, \quad (30)$$

where $a \approx 3.847 \times 10^8$ m and $e \approx 0.055$ are the initial values of the semimajor axis and eccentricity of the Moon's elliptical orbit, respectively. When the observation point is at perigee, namely, $\varphi = 0$, we have

$$\frac{1-e^2}{1+e\cos f} \approx 1, \quad (31)$$

$$\frac{-2e(1+e\cos f)-(1-e^2)\cos f}{(1+e\cos f)^2} \approx -1. \quad (32)$$

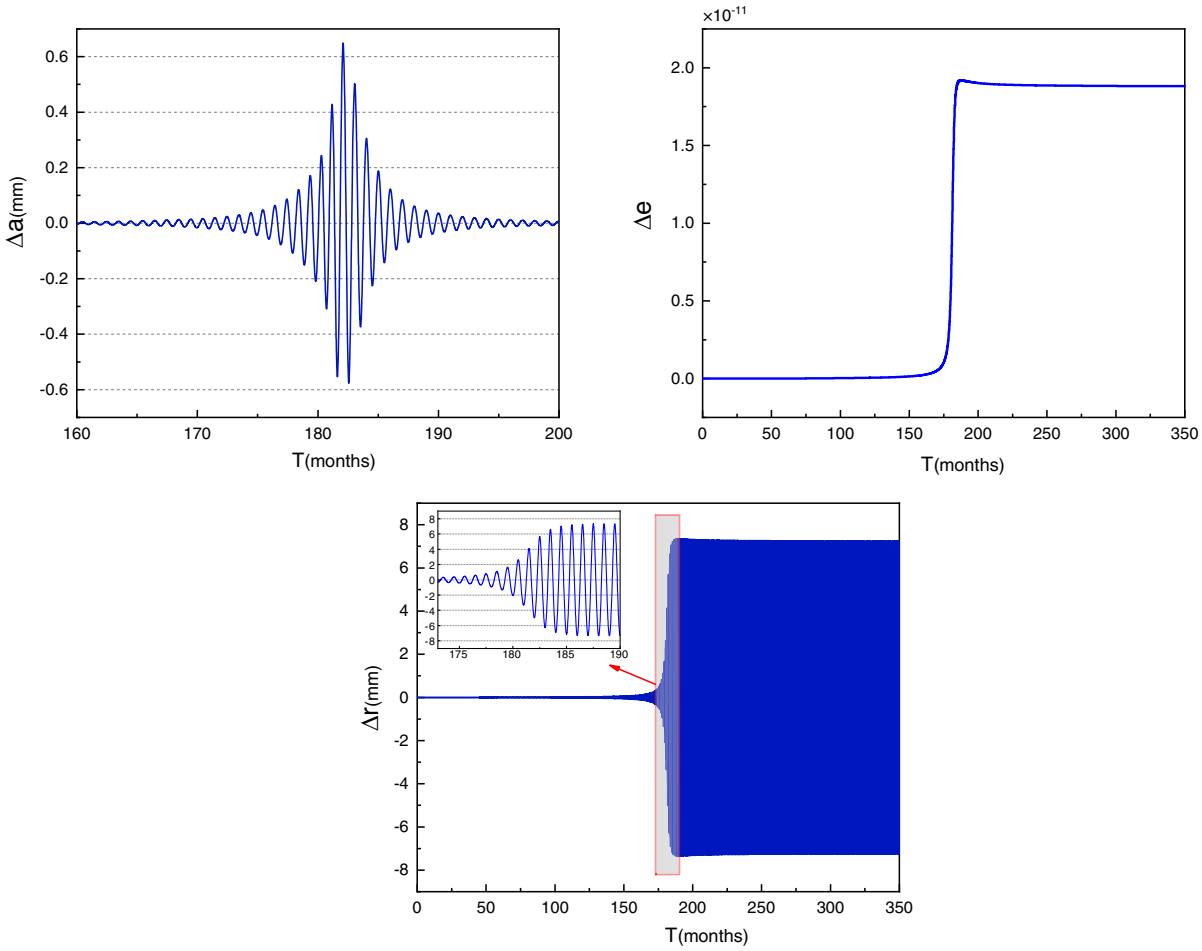

FIG. 11. Evolution of Δa, Δe, Δr with time.

Then

$$\Delta r \approx \Delta a - a\Delta e. \tag{33}$$

Comparing Fig. 11, one can see that the magnitude of Δa is much smaller than the term $a\Delta e$, therefore Δr is mainly determined by Δe.

The evolution of Δr with time under different observation angles φ and the dependence of Δr on φ are shown in Fig. 12. From the right plane of Fig. 12, one can see that the long-term effects of the perturbing force of PBH on the Earth-Moon distance are different under different observation angles. Combining the right plane of Figs. 5 and 12, one can further see that the dependence of Δr on φ is the same when i, Ω and ω take different initial values. This means that Δr always acts as a cosine function of φ, no matter where the orientation of the PBH is relative to the Earth-Moon binary system.

The effects of the perturbing force of PBH on the Earth-Moon binary system under different azimuths, distances and masses of the PBH, which is equivalent to varying one of the parameters i, Ω, ω, b, m_2 and let other parameters fixed, are shown in the left panels of Figs. 13–17, respectively. The dependences of Δr on i, Ω, ω, b, m_2, on the other hand, are shown in the right panels of Figs. 13–17, respectively.

From these figures, one can see that Δr is insensitive to Ω when $c(t) = 100b$, comparing to i and ω, whose changes would have larger effects on Δr. In the coplanar case we see the same behavior. Comparing the right panels of Figs. 8 and 15, one can see that Δr always acts as a cosine function of ω, regardless of whether the PBH and the elliptical orbit of the Moon are coplanar or not. In addition, Δr can always return to zero, as long as the value of ω is $\frac{\pi}{2}$ or $\frac{3\pi}{2}$, no matter what the values of i and Ω are. This point can be understood as follows. First, the elliptical orbit of the Moon is perfectly symmetrical about the Z axis when the value of ω is $\frac{\pi}{2}$ or $\frac{3\pi}{2}$. Additionally, the trajectory of the PBH is symmetrical about the Z axis. This results in the work done by the perturbing force of PBH being equal to zero over the process. So the perturbing force of the PBH will not have long-term effects on the Earth-Moon binary system when the initial value of ω is $\frac{\pi}{2}$ or $\frac{3\pi}{2}$, no matter what the initial values of i and Ω are. Combining Figs. 9, 10, 16, and 17,

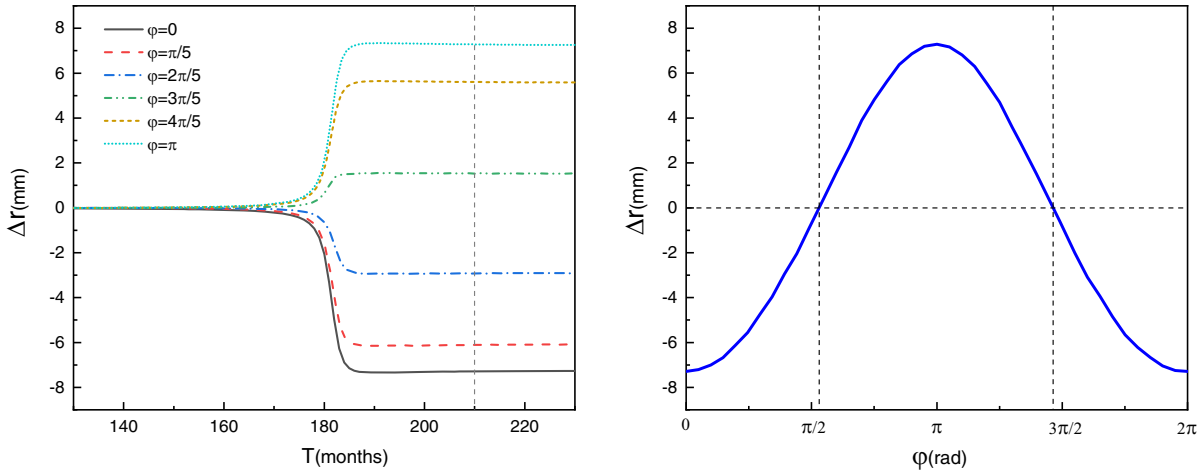

FIG. 12. Left panel: evolution of Δr with time under different fixed observation angles φ. Right panel: the values of $\Delta r(T = 210)$ at the dotted line in the figure on the left panel as a function of φ, which corresponds to the dependence of Δr on φ when $c(t) = 100b$.

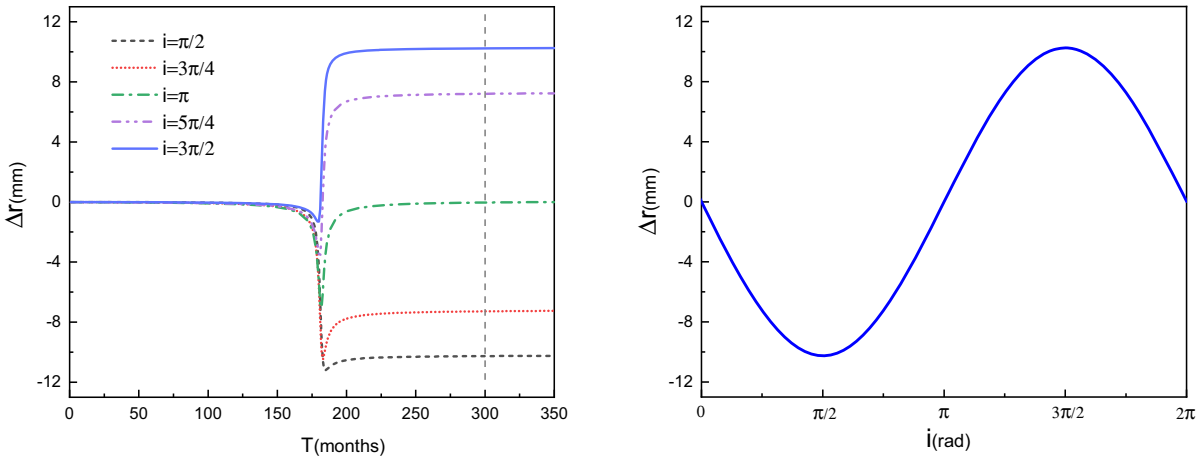

FIG. 13. Left panel: evolution of Δr with time when $\varphi = 0$ under different i and other parameters fixed. Right panel: the values of $\Delta r(T = 300)$ at the dotted line in the figure on the left panel as a function of i, which corresponds to the dependence of Δr on i when $c(t) = 100b$.

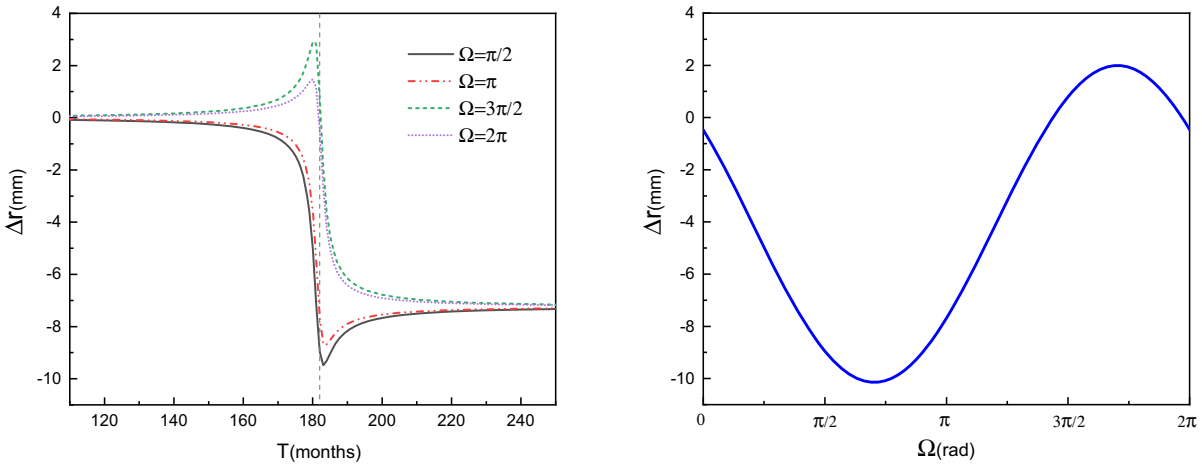

FIG. 14. Left panel: the evolution of Δr with time when $\varphi = 0$ under different Ω and other parameters fixed. Right panel: the values of $\Delta r(T = 182)$ at the dotted line in the figure on the left panel as a function of Ω, which corresponds to the dependence of Δr on Ω when $c(t) = 0$.

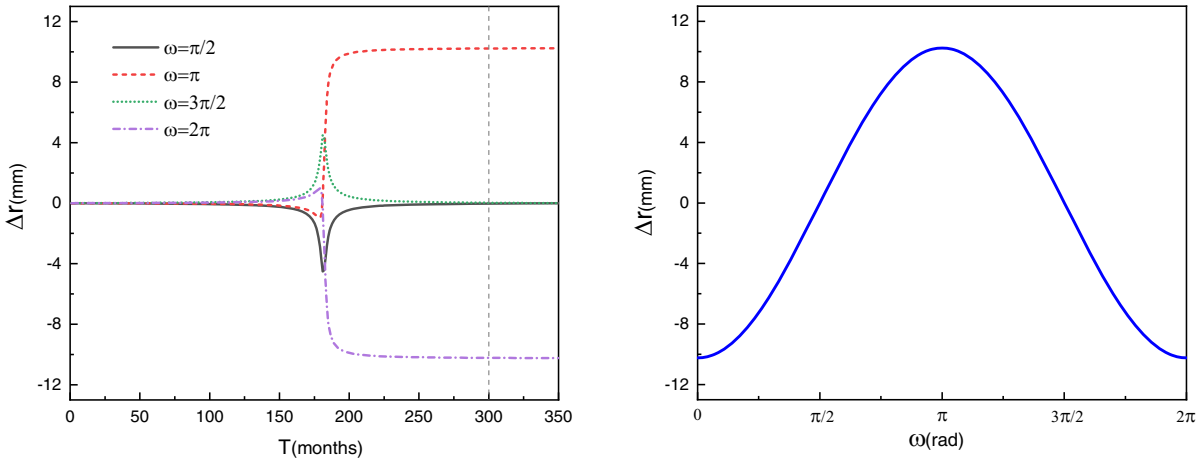

FIG. 15. Left panel: the evolution of Δr with time when $\varphi = 0$ under different ω and other parameters fixed. Right panel: the values of $\Delta r(T = 300)$ at the dotted line in the figure on the left panel as a function of ω, which corresponds to the dependence of Δr on ω when $c(t) = 100b$.

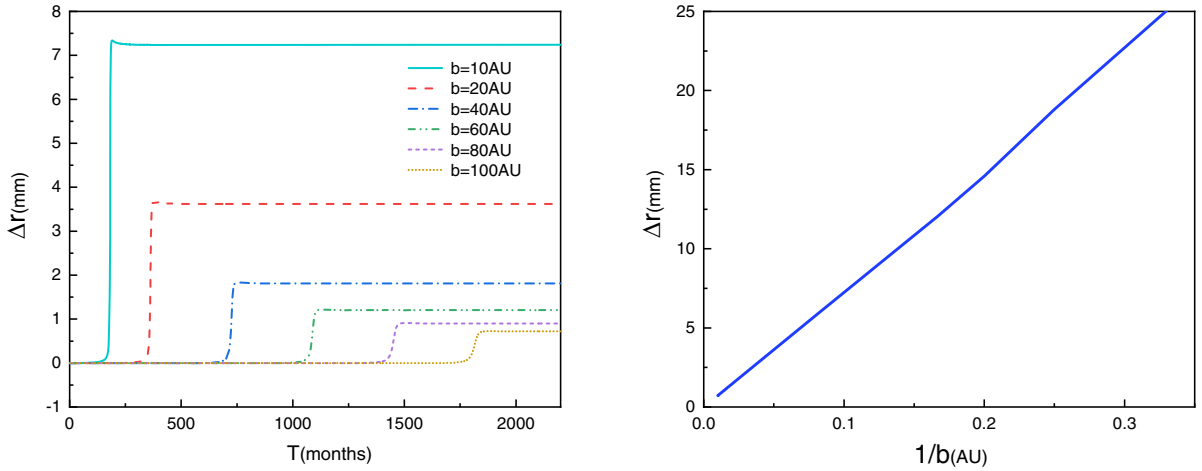

FIG. 16. Left panel: evolution of Δr with time when $\varphi = \pi$ under different b and other parameters fixed. Right panel: the dependence of Δr on $\frac{1}{b}$ when $c(t) = 100b$.

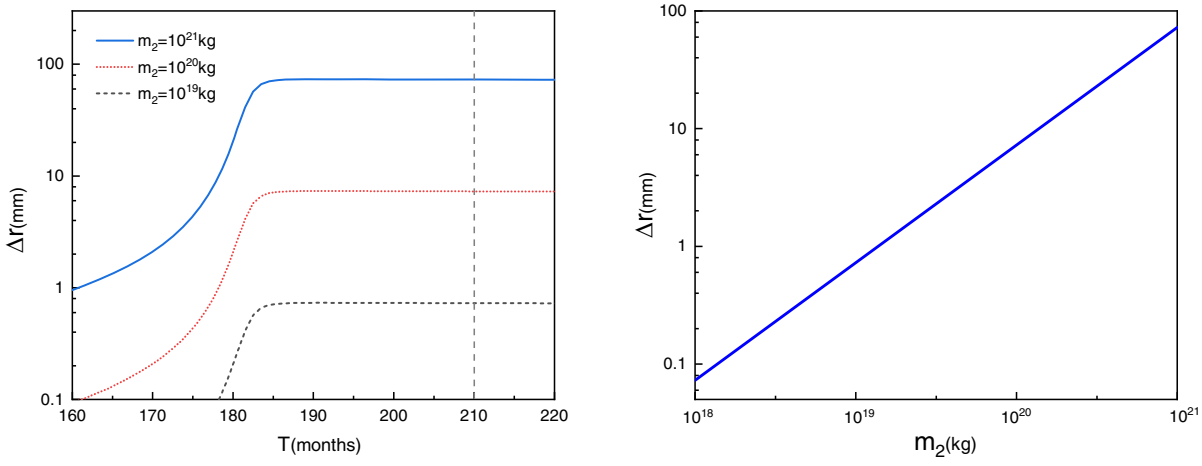

FIG. 17. Left panel: evolution of Δr with time when $\varphi = \pi$ under different m_2. Right panel: the values of $\Delta r(T = 210)$ at the dotted line in the figure on the left panel as a function of m_2, which corresponds to the dependence of Δr on m_2 when $c(t) = 100b$.

one can see that the dependence of Δr on b or m_2 is the same, regardless of whether the initial position of the PBH is coplanar with the Earth-Moon binary system or not.

It is worth noting that in most cases, the values of Δr are within the sensitivity of the current observations, such as the lunar laser ranging (LLR), whose normal point measurement can determine the Earth-Moon distance to as precise as 1 mm [92]. That is to say, taking $b = 10$ AU and $c(t) = 100b$ as an example, signals for PBHs with mass larger than 10^{19} kg should be able to detect by the normal point measurement.

V. CONCLUSIONS AND DISCUSSIONS

In summary, we give a new proposal which can be used to detect sublunar-mass PBHs. In addition, by treating PBH as a perturbative term, we develop a framework to calculate the orbits of a generic binary system such as the Earth-Moon binary system. In order for the perturbative calculations to be trustable, one needs to assume that the PBH is far away from the Earth-Moon binary (far greater than 1 AU); the mass of the PBH should be less than the Moon. These requirements constrain that the motivated PBH should have the mass less than 10^{22} kg, a sublunar-mass PBH.

Our numerical results show that the Earth-Moon distance is sensitive to the initial values of the system. Our discussion divides into two cases. One is for the case where the initial position of the PBH is coplanar to the Earth-Moon binary system, the other is the opposite, i.e., the PBH is noncoplanar to the Earth-Moon binary. Both cases exhibit many similar behaviors. For example, in both cases, the Earth-Moon distance difference between with and without PBH Δr always acts as a cosine function of φ, and $|\Delta r|$ reaches its maximum value when φ is equal to 0 or π, which means that the greatest change in the distance between the Earth and the Moon can be observed by the normal point measurement. Similarly, in both cases, Δr acts as a trigonometric function of i, ω and Ω, and there always have been long-term effects to the Earth-Moon orbits except for the case with $\omega = \frac{\pi}{2}, \frac{3\pi}{2}$, no matter what the initial values of other parameters are. Also, the long-term effects to the Earth-Moon orbits are insensitive to the initial value of Ω, comparing to those of i and ω, whose initial values would have a significant impact on the long-term effects. In addition, we observe the similar behavior of Δr varying with the distance b in both cases. The peak value of Δr gradually decreases as b increases, which means that the further the PBH from the Earth-Moon binary system is, the smaller the offset of the Moon's elliptical orbit will be. Our results also show that Δr is proportional to m_2, which is consistent with the calculated results in Refs. [94,95]. Therefore, the greater the mass of the PBH is, the greater the offset of the Moon's elliptical orbit will be.

Our results provide strong motivation for further work to develop the binary system as an accurate measurement tool for sublunar-mass PBHs. It is of great interest to develop some data analysis pipelines to conduct PBH searches with laser-ranging data, such that one can efficiently study the sublunar-mass PBHs, and put new observational constraints on searching these sublunar-mass PBHs. Furthermore, we can extend our analysis to investigate the impact of PBHs on other binary systems, such as the Sun-Mercury and Sun-Mars binary systems. As a concrete example, let us consider the impact of PBHs on the Sun-Mercury system. To do this, we first substitute the initial value of Mercury's orbit into our setup, choose the initial conditions as $\mathrm{i} = \frac{\pi}{2}$, $\Omega = \frac{\pi}{2}$, $\omega = \frac{\pi}{2}$, $\mathrm{b} = 100$ AU, $\mathrm{m}_2 = 10^{22}$ kg, and then follow the methodology presented in this paper. Finally, we find that the deviation of Mercury's orbit caused by PBH perturbations is approximately 20 cm. With current measurement accuracy of the distance between Earth and Mercury at approximately 20 cm [96], monitoring the distance between Earth and Mercury may provide a means to detect PBHs.

In this work, we focused on the effects of a single PBH sweeping past the Solar System. However, it is also interesting to investigate the effects of multiple PBHs with different masses passing close to the Earth-Moon system. To see the possibility of this phenomena, let us estimate the upper bound on the expected rate of two PBHs sweeping past the Solar System simultaneously. To estimate the event rate, we first consider the fraction of dark matter in the form of PBHs, denoted as $f_{PBH} = \frac{\rho_{PBH}}{\rho_{\mathrm{DM}}}$. For a given mass, the event rate P of a PBH sweeping past the Solar System with a radius of 100 AU can be calculated using the following equation [94]:

$$P = 0.1607\ \mathrm{yr}^{-1} \cdot \frac{f_{\mathrm{PBH}}}{1.0} \cdot \frac{\rho_{\mathrm{DM}}}{0.3\ \mathrm{GeV} \cdot \mathrm{cm}^{-3}} \cdot \frac{v}{350\ \mathrm{km} \cdot \mathrm{s}^{-1}} \cdot \frac{10^{20}\ \mathrm{kg}}{M_{\mathrm{PBH}}} \cdot \left(\frac{b}{100\ \mathrm{AU}}\right)^2. \tag{34}$$

From the equation, we can see that the event rate P is $0.1607\ \mathrm{yr}^{-1}$ for a PBH with a mass of 10^{20} kg, a distance of $b = 100$ AU, a velocity of $v = 350\ \mathrm{km} \cdot \mathrm{s}^{-1}$ [53], and the assumption that all dark matter is composed of PBHs with a certain mass, i.e., $f_{\mathrm{PBH}} = 1$. Based on this estimation, we roughly get that the probability of two PBHs with a mass of 10^{20} kg sweeping past the Solar System simultaneously is about $0.0258\ \mathrm{yr}^{-1}$. Therefore, investigating the effects of multiple PBHs passing close to the Earth-Moon system is a promising avenue for future research.

As a future work, it is also of great interest to extend our model to analyze the relationship between f_{PBH} and M_{PBH} in Eq. (34) to study the signatures in the usual plane

abundance vs PBH mass. This can be done under the assumption that M_{PBH} is monochromatic. Simply put, as suggested in our work, the observed quantity Δr is proportional to m_{PBH} and inversely proportional to b, that is, $\Delta r \sim \frac{M_{\mathrm{PBH}}}{b}$. Substituting this into Eq. (34), we obtain

$$f_{\mathrm{PBH}} \sim \frac{P \cdot \triangle r^2}{\rho_{\mathrm{DM}} \cdot v \cdot M_{\mathrm{PBH}}}. \tag{35}$$

Since ρ_{DM} and v are known quantities, and P and Δr are observed quantities in Eq. (35), f_{PBH} is inversely proportional to M_{PBH}. This means that it will be possible to obtain new bounds on PBH DM with a monochromatic mass distribution.

ACKNOWLEDGMENTS

This work is partially supported by the National Natural Science Foundation of China with Grant No. 11975116.

[1] G. Bertone and D. Hooper, History of dark matter, Rev. Mod. Phys. **90**, 045002 (2018).
[2] N. Aghanim *et al.*, Planck 2018 results. VI. Cosmological parameters, Astron. Astrophys. **641**, A6 (2020); **652**, C4(E) (2021).
[3] D. Clowe, M. Bradac, A. H. Gonzalez, M. Markevitch, S. W. Randall, C. Jones, and D. Zaritsky, A direct empirical proof of the existence of dark matter, Astrophys. J. Lett. **648**, L109 (2006).
[4] Y. Sofue and V. Rubin, Rotation curves of spiral galaxies, Annu. Rev. Astron. Astrophys. **39**, 137 (2001).
[5] G. Arcadi, M. Dutra, P. Ghosh, M. Lindner, Y. Mambrini, M. Pierre, S. Profumo, and F. S. Queiroz, The waning of the WIMP? A review of models, searches, and constraints, Eur. Phys. J. C **78**, 203 (2018).
[6] L. Roszkowski, E. M. Sessolo, and S. Trojanowski, WIMP dark matter candidates and searches—Current status and future prospects, Rep. Prog. Phys. **81**, 066201 (2018).
[7] Y. B. Zeldovich and I. D. Novikov, The hypothesis of cores retarded during expansion and the hot cosmological model. Soviet Astron. AJ (Engl. Transl.) **10**, 602 (1967).
[8] S. Hawking, Gravitationally collapsed objects of very low mass, Mon. Not. R. Astron. Soc. **152**, 75 (1971).
[9] B. J. Carr and S. W. Hawking, Black holes in the early Universe, Mon. Not. R. Astron. Soc. **168**, 399 (1974).
[10] B. J. Carr, The primordial black hole mass spectrum, Astrophys. J. **201**, 1 (1975).
[11] S. W. Hawking, Black holes from cosmic strings, Phys. Lett. B **231**, 237 (1989).
[12] A. Polnarev and R. Zembowicz, Formation of primordial black holes by cosmic strings, Phys. Rev. D **43**, 1106 (1991).
[13] J. Yokoyama, Formation of macho-primordial black holes in inflationary cosmology, Astron. Astrophys. **318**, 673 (1997).
[14] J. Garcia-Bellido, A. Linde, and D. Wands, Density perturbations and black hole formation in hybrid inflation, Phys. Rev. D **54**, 6040 (1996).
[15] J. C. Niemeyer and K. Jedamzik, Near-Critical Gravitational Collapse and the Initial Mass Function of Primordial Black Holes, Phys. Rev. Lett. **80**, 5481 (1998).
[16] S. Clesse and J. García-Bellido, Massive primordial black holes from hybrid inflation as dark matter and the seeds of galaxies, Phys. Rev. D **92**, 023524 (2015).
[17] J. Garriga, A. Vilenkin, and J. Zhang, Black holes and the multiverse, J. Cosmol. Astropart. Phys. 02 (2016) 064.
[18] H. Deng, J. Garriga, and A. Vilenkin, Primordial black hole and wormhole formation by domain walls, J. Cosmol. Astropart. Phys. 04 (2017) 050.
[19] J. Garcia-Bellido and E. R. Morales, Primordial black holes from single field models of inflation, Phys. Dark Universe **18**, 47 (2017).
[20] B.-M. Gu, F.-W. Shu, K. Yang, and Y.-P. Zhang, Primordial black holes from valley, Phys. Rev. D **107**, 023519 (2023).
[21] Y.-F. Cai, X.-H. Ma, M. Sasaki, D.-G. Wang, and Z. Zhou, One small step for an inflaton, one giant leap for inflation: A novel non-Gaussian tail and primordial black holes, Phys. Lett. B **834**, 137461 (2022).
[22] Y.-F. Cai, X. Tong, D.-G. Wang, and S.-F. Yan, Primordial Black Holes from Sound Speed Resonance During Inflation, Phys. Rev. Lett. **121**, 081306 (2018).
[23] C. Chen, X.-H. Ma, and Y.-F. Cai, Dirac-Born-Infeld realization of sound speed resonance mechanism for primordial black holes, Phys. Rev. D **102**, 063526 (2020).
[24] C. Fu, P. Wu, and H. Yu, Primordial black holes from inflation with nonminimal derivative coupling, Phys. Rev. D **100**, 063532 (2019).
[25] J. Lin, Q. Gao, Y. Gong, Y. Lu, C. Zhang and F. Zhang *et al.*, Primordial black holes and secondary gravitational waves from k and g inflation, Phys. Rev. D **101**, 103515 (2020).
[26] Z. Yi, Q. Gao, Y. Gong, and Z. H. Zhu, Primordial black holes and scalar-induced secondary gravitational waves from inflationary models with a noncanonical kinetic term, Phys. Rev. D **103**, 063534 (2021).
[27] Z. Yi, Y. Gong, B. Wang, and Z. H. Zhu, Primordial black holes and secondary gravitational waves from the Higgs field, Phys. Rev. D **103**, 063535 (2021).
[28] Q. Gao, Y. Gong, and Z. Yi, Primordial black holes and secondary gravitational waves from natural inflation, Nucl. Phys. **B969**, 115480 (2021).
[29] Q. Gao, Primordial black holes and secondary gravitational waves from chaotic inflation, Sci. China Phys. Mech. Astron. **64**, 1 (2021).
[30] C. Fu, P. Wu, and H. Yu, Primordial black holes and oscillating gravitational waves in slow-roll and slow-climb inflation with an intermediate noninflationary phase, Phys. Rev. D **102**, 043527 (2020).

[31] D.-S. Meng, C. Yuan, and Q.-G. Huang, One-loop correction to the enhanced curvature perturbation with local-type non-Gaussianity for the formation of primordial black holes, Phys. Rev. D **106**, 063508 (2022).
[32] Z. Zhou, J. Jiang, Y.-F. Cai, M. Sasaki, and S. Pi, Primordial black holes and gravitational waves from resonant amplification during inflation, Phys. Rev. D **102**, 103527 (2020).
[33] R.-G. Cai, Z.-K. Guo, J. Liu, L. Liu, and X.-Y. Yang, Primordial black holes and gravitational waves from parametric amplification of curvature perturbations, J. Cosmol. Astropart. Phys. 06 (2020) 013.
[34] R.-G. Cai, C. Chen, and C. Fu, Primordial black holes and stochastic gravitational wave background from inflation with a noncanonical spectator field, Phys. Rev. D **104**, 083537 (2021).
[35] L. Wu, Y. Gong, T. Li *et al.*, Primordial black holes and secondary gravitational waves from string inspired general no-scale supergravity, Phys. Rev. D **104**, 123544 (2021).
[36] H. Di and Y. Gong, Primordial black holes and second order gravitational waves from ultra-slow-roll inflation, J. Cosmol. Astropart. Phys. 07 (2018) 007.
[37] C. Chen and Y.-F. Cai, Primordial black holes from sound speed resonance in the inflaton-curvaton mixed scenario, J. Cosmol. Astropart. Phys. 10 (2019) 068.
[38] M. Y. Khlopov, Primordial black holes, Res. Astron. Astrophys. **10**, 495 (2010).
[39] K. Belotsky, A. Dmitriev, E. Esipova, V. Gani, A. Grobov, M. Y. Khlopov, A. Kirillov, S. Rubin, and I. Svadkovsky, Signatures of primordial black hole dark matter, Mod. Phys. Lett. A **29**, 1440005 (2014).
[40] K. M. Belotsky, V. I. Dokuchaev, Y. N. Eroshenko, E. A. Esipova, M. Y. Khlopov, L. A. Khromykh, A. A. Kirillov, V. V. Nikulin, S. G. Rubin, and I. V. Svadkovsky, Clusters of primordial black holes, Eur. Phys. J. C **79**, 1 (2019).
[41] S. V. Ketov and M. Y. Khlopov, Cosmological probes of supersymmetric field theory models at superhigh energy scales, Symmetry **11**, 511 (2019).
[42] S. Pi, Y.-l. Zhang, Q.-G. Huang, and M. Sasaki, Scalaron from r2-gravity as a heavy field, J. Cosmol. Astropart. Phys. 05 (2018) 042.
[43] R. Abbott *et al.*, GW190521: A Binary Black Hole Merger with a Total Mass of $150M_{\odot}$, Phys. Rev. Lett. **125**, 101102 (2020).
[44] R. Abbott *et al.*, Properties and astrophysical implications of the $150M_{\odot}$ binary black hole merger GW190521, Astrophys. J. Lett. **900**, L13 (2020).
[45] A. Katz, J. Kopp, S. Sibiryakov, and W. Xue, Femtolensing by dark matter revisited, J. Cosmol. Astropart. Phys. 12 (2018) 005.
[46] J. B. Muñoz, E. D. Kovetz, L. Dai, and M. Kamionkowski, Lensing of Fast Radio Bursts as a Probe of Compact Dark Matter, Phys. Rev. Lett. **117**, 091301 (2016).
[47] S. Jung and C. S. Shin, Gravitational-Wave Fringes at LIGO: Detecting Compact Dark Matter by Gravitational Lensing, Phys. Rev. Lett. **122**, 041103 (2019).
[48] S. Jung and T. H. Kim, Gamma-ray burst lensing parallax: Closing the primordial black hole dark matter mass window, Phys. Rev. Res. **2**, 013113 (2020).
[49] R. Laha, Lensing of fast radio bursts: Future constraints on primordial black hole density with an extended mass function and a new probe of exotic compact fermion and boson stars, Phys. Rev. D **102**, 023016 (2020).
[50] B. P. Abbott *et al.*, Observation of Gravitational Waves from a Binary Black Hole Merger, Phys. Rev. Lett. **116**, 061102 (2016).
[51] B. P. Abbott *et al.*, Binary black hole population properties inferred from the first and second observing runs of Advanced LIGO and Advanced Virgo, Astrophys. J. Lett. **882**, L24 (2019).
[52] C. Alcock *et al.*, The MACHO project: Microlensing results from 5.7 years of LMC observations, Astrophys. J. **542**, 281 (2000).
[53] B. J. Carr and M. Sakellariadou, Dynamical constraints on dark matter in compact objects, Astrophys. J. **516**, 195 (1999).
[54] N. Afshordi, P. McDonald, and D. N. Spergel, Primordial black holes as dark matter: The power spectrum and evaporation of early structures, Astrophys. J. Lett. **594**, L71 (2003).
[55] B. J. Carr, K. Kohri, Y. Sendouda, and J. Yokoyama, New cosmological constraints on primordial black holes, Phys. Rev. D **81**, 104019 (2010).
[56] B. Carr, F. Kuhnel, and M. Sandstad, Primordial black holes as dark matter, Phys. Rev. D **94**, 083504 (2016).
[57] B. Carr, M. Raidal, T. Tenkanen, V. Vaskonen, and H. Veermäe, Primordial black hole constraints for extended mass functions, Phys. Rev. D **96**, 023514 (2017).
[58] V. Poulin, P. D. Serpico, F. Calore, S. Clesse, and K. Kohri, CMB bounds on disk-accreting massive primordial black holes, Phys. Rev. D **96**, 083524 (2017).
[59] B. Carr, K. Kohri, Y. Sendouda, and J. Yokoyama, Constraints on primordial black holes, Rep. Prog. Phys. **84**, 116902 (2021).
[60] M. Sasaki, T. Suyama, T. Tanaka, and S. Yokoyama, Primordial black holes—Perspectives in gravitational wave astronomy, Classical Quantum Gravity **35**, 063001 (2018).
[61] A. M. Green and B. J. Kavanagh, Primordial black holes as a dark matter candidate, J. Phys. G **48**, 043001 (2021).
[62] P. Tisserand *et al.*, Limits on the Macho content of the galactic halo from the EROS-2 survey of the magellanic clouds, Astron. Astrophys. **469**, 387 (2007).
[63] Y. Ali-Haïmoud and M. Kamionkowski, Cosmic microwave background limits on accreting primordial black holes, Phys. Rev. D **95**, 043534 (2017).
[64] P. D. Serpico, V. Poulin, D. Inman, and K. Kohri, Cosmic microwave background bounds on primordial black holes including dark matter halo accretion, Phys. Rev. Res. **2**, 023204 (2020).
[65] G. Hütsi, M. Raidal, and H. Veermäe, Small-scale structure of primordial black hole dark matter and its implications for accretion, Phys. Rev. D **100**, 083016 (2019).
[66] S. Wang, Y.-F. Wang, Q.-G. Huang, and T. G. F. Li, Constraints on the Primordial Black Hole Abundance from the First Advanced LIGO Observation Run Using the Stochastic Gravitational-Wave Background, Phys. Rev. Lett. **120**, 191102 (2018).
[67] S. Bird, I. Cholis, J. B. Muñoz, Y. Ali-Haïmoud, M. Kamionkowski, E. D. Kovetz, A. Raccanelli, and A. G. Riess, Did LIGO Detect Dark Matter?, Phys. Rev. Lett. **116**, 201301 (2016).

[68] S. M. Koushiappas and A. Loeb, Dynamics of Dwarf Galaxies Disfavor Stellar-Mass Black Holes as Dark Matter, Phys. Rev. Lett. **119**, 041102 (2017).
[69] T. D. Brandt, Constraints on MACHO dark matter from compact stellar systems in ultra-faint dwarf galaxies, Astrophys. J. Lett. **824**, L31 (2016).
[70] Y.-F. Wang, Q.-G. Huang, T. G. F. Li, and S. Liao, Searching for primordial black holes with stochastic gravitational-wave background in the space-based detector frequency band, Phys. Rev. D **101**, 063019 (2020).
[71] M. Sasaki, T. Suyama, T. Tanaka, and S. Yokoyama, Primordial Black Hole Scenario for the Gravitational-Wave Event GW150914, Phys. Rev. Lett. **117**, 061101 (2016).
[72] Y. Ali-Haïmoud, E. D. Kovetz, and M. Kamionkowski, Merger rate of primordial black-hole binaries, Phys. Rev. D **96**, 123523 (2017).
[73] V. De Luca, G. Franciolini, P. Pani, and A. Riotto, Primordial black holes confront LIGO/Virgo data: Current situation, J. Cosmol. Astropart. Phys. 06 (2020) 044.
[74] K. Jedamzik, Primordial black hole dark matter and the LIGO/Virgo observations, J. Cosmol. Astropart. Phys. 09 (2020) 022.
[75] K. Jedamzik, Consistency of Primordial Black Hole Dark Matter with LIGO/Virgo Merger Rates, Phys. Rev. Lett. **126**, 051302 (2021).
[76] B. Dasgupta, R. Laha, and A. Ray, Neutrino and Positron Constraints on Spinning Primordial Black Hole Dark Matter, Phys. Rev. Lett. **125**, 101101 (2020).
[77] L. Chen, Q.-G. Huang, and K. Wang, Constraint on the abundance of primordial black holes in dark matter from Planck data, J. Cosmol. Astropart. Phys. 12 (2016) 044.
[78] R. Kimura, T. Suyama, M. Yamaguchi, and Y.-l. Zhang, Reconstruction of primordial power spectrum of curvature perturbation from the merger rate of primordial black hole binaries, J. Cosmol. Astropart. Phys. 04 (2021) 031.
[79] X. Wang, Y.-l. Zhang, R. Kimura, and M. Yamaguchi, Reconstruction of power spectrum of primordial curvature perturbations on small scales from primordial black hole binaries scenario of LIGO/Virgo detection, Sci. China Phys. Mech. Astron. **66**, 260462 (2023).
[80] F. Capela, M. Pshirkov, and P. Tinyakov, Constraints on primordial black holes as dark matter candidates from star formation, Phys. Rev. D **87**, 023507 (2013).
[81] F. Capela, M. Pshirkov, and P. Tinyakov, Constraints on primordial black holes as dark matter candidates from capture by neutron stars, Phys. Rev. D **87**, 123524 (2013).
[82] F. Capela, M. Pshirkov, and P. Tinyakov, Adiabatic contraction revisited: Implications for primordial black holes, Phys. Rev. D **90**, 083507 (2014).
[83] N. Esser and P. Tinyakov, Constraints on primordial black holes from observation of stars in dwarf galaxies, arXiv:2207.07412.
[84] D. Brouwer and G. M. Clemence, *Methods of Celestial Mechanics* (Elsevier, New York, 2013).
[85] J. A. Burns, Elementary derivation of the perturbation equations of celestial mechanics, Am. J. Phys. **44**, 944 (1976).
[86] L. Hui, S. T. McWilliams, and I. S. Yang, Binary systems as resonance detectors for gravitational waves, Phys. Rev. D **87**, 084009 (2013).
[87] E. Poisson and C. M. Will, *Gravity: Newtonian, Post-Newtonian, Relativistic* (Cambridge University Press, Cambridge, England, 2014).
[88] C. D. Murray and S. F. Dermott, *Solar System Dynamics* (Cambridge University Press, Cambridge, England, 1999).
[89] T. Murphy, E. G. Adelberger, J. Battat, L. Carey, C. D. Hoyle, LeBlanc, E. Michelsen, K. Nordtvedt, A. Orin, J. D. Strasburg *et al.*, The apache point observatory lunar laser-ranging operation: Instrument description and first detections, Publ. Astron. Soc. Pac. **120**, 20 (2008).
[90] J. B. Battat, T. Murphy, E. G. Adelberger, B. Gillespie, C. Hoyle, R. McMillan, E. L. Michelsen, K. Nordtvedt, A. E. Orin, C. W. Stubbs *et al.*, The apache point observatory lunar laser-ranging operation (APOLLO): Two years of millimeter-precision measurements of the earth-moon range[1], Publ. Astron. Soc. Pac. **121**, 29 (2009).
[91] T. Murphy, E. Adelberger, J. Battat, C. Hoyle, N. Johnson, R. McMillan, C. Stubbs, and H. Swanson, Apollo: Millimeter lunar laser ranging, Classical Quantum Gravity **29**, 184005 (2012).
[92] T. Murphy, Lunar laser ranging: The millimeter challenge, Rep. Prog. Phys. **76**, 076901 (2013).
[93] M. Du, Q. Deng, Y. Bian, Z. Luo, and P. Xu, Probing supermassive black hole binaries with orbital resonances of laser-ranged satellite, arXiv:2207.01100.
[94] N. Seto and A. Cooray, Searching for primordial black hole dark matter with pulsar timing arrays, Astrophys. J. **659**, L33 (2007).
[95] K. Kashiyama and N. Seto, Enhanced exploration for primordial black holes using pulsar timing arrays, Mon. Not. R. Astron. Soc. **426**, 1369 (2012).
[96] J. F. Cavanaugh, J. C. Smith, X. Sun, A. E. Bartels, L. Ramos-Izquierdo, D. J. Krebs, J. F. McGarry, R. Trunzo, A. M. Novo-Gradac, J. L. Britt *et al.*, The mercury laser altimeter instrument for the messenger mission, Space Sci. Rev. **131**, 451 (2007).